Inorganic Chemistry

Article

pubs.acs.org/IC

$AAg_2(M'_{1/3}M_{2/3})[VO_4]_2$: Synthesis, Magnetic Properties, and Lattice Dynamics of Honeycomb-Type Lattices

Michaela Bratsch,[†] Joshua Tapp,[†] Alexander P. Litvinchuk,[‡] and Angela Möller*[,†]

[†]Department of Chemistry and Texas Center for Superconductivity, University of Houston, Houston, Texas 77204-5003, United States

[‡]Texas Center for Superconductivity and Department of Physics, University of Houston, Houston, Texas 77204-5002, United States

Supporting Information

ABSTRACT: The magnetic honeycomb lattice series of compounds, $AAg_2(M'_{1/3}M_{2/3})[VO_4]_2$ with A = Ba^{2+}, Sr^{2+}, M′ = Mg^{2+}, Zn^{2+}, and M = Mn^{2+}, Co^{2+}, and Ni^{2+}, have been synthesized and their physical properties are reported. This series of compounds contains the M′ and M cations in a 1:2 ratio on a single crystallographic site. In an ordered arrangement, this could generate a magnetic honeycomb-type lattice. Presented X-ray diffraction data, spectroscopic measurements of lattice dynamics, along with ab initio calculations, magnetic, and specific heat data for these compounds clearly point toward the formation of magnetic honeycomb-type lattices.

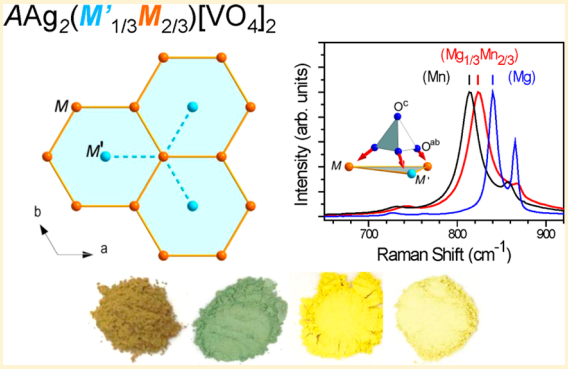

1. INTRODUCTION

In solid state chemistry, an important area of research is related to structure−property relationships of compounds. Compounds with different two-dimensional (2D) magnetic lattices, i.e., triangular lattices,[1−5] honeycomb lattices,[6−16] and Kagome lattices[17,18] have been identified to exhibit many intriguing properties. An important and interesting aspect of low-dimensional compounds relates to superexchange pathways between magnetic ions via nonmagnetic ligands (e.g., O^{2-}) or complex units like $[VO_4]^{3-}$. This can be described by a super exchange (SE),[19−21] i.e., *M*—O—*M*, or by a supersuper exchange (SSE),[22−24] i.e., *M*—O−V−O—*M*. Two-dimensional layered compounds of the type, $AAg_2M[VO_4]_2$[1−4] and $ANa_2M[VO_4]_2$[5] contain magnetic metal ions (M) on a triangular lattice, where magnetic ions are linked via the nonmagnetic $[VO_4]^{3-}$ unit. The magnetic SSE between the cations on the M-site is mediated by the vanadate unit here. The different magnetic triangular lattices that have been studied earlier are Mn^{2+}, Co^{2+}, Ni^{2+}, and Cu^{2+} representing different spin-systems with *S* = 5/2, 3/2, 1, and 1/2, respectively. The Co^{2+} and Ni^{2+} compounds have been shown to be ferromagnetic insulators,[1,3] while the Mn^{2+} compounds exhibit instead an antiferromagnetic behavior.[3] The $BaAg_2Mn[VO_4]_2$ compound is an example for the realization of frustrated triangular lattice antiferromagnet.[3] The Cu^{2+} compound is interesting because both ferromagnetic and antiferromagnetic interactions in one dimension (chain) are present and result in an intriguing behavior of their thermodynamic properties.[2,4] For further work on nontrivial ground states in low-dimensional spin-systems, see for example refs 24−26.

There are many possible variations of the triangular lattices; one of these is the honeycomb lattice. A magnetic honeycomb lattice occurs when the M-site metals on the triangular lattice are replaced in a 1:2 ratio of nonmagnetic metals to magnetic metals. It is expected that the physical properties change according to the number of nearest magnetic neighbors, which is reduced from six to three per magnetic site. Magnetic honeycomb lattices have been shown to exhibit interesting properties like spin-flop,[6] helimagnetism,[7] superconductivity,[8] and spin-glass behavior.[9] Previously synthesized and characterized honeycomb compounds took advantage of charge and size differences of cations to facilitate the creation of a well ordered honeycomb lattice (at least on the scale related to the respective correlation lengths). Examples are $Li_3Ni_2BiO_6$[10] with a honeycomb-type of ordering between the Ni^{2+} and the Bi^{5+}, or $InCu_{2/3}V_{1/3}O_3$[11−13] with respect to Cu^{2+} and V^{5+}. Another series of compounds that has been studied in detail is $BaNi_2X_2O_8$ with X = P, As, and V,[14−16] where solely Ni^{2+} ions form a honeycomb arrangement with the central site remaining unoccupied.

The focus of this research is to report the synthesis of a novel series of compounds that contain magnetic transition metal ions arranged in a honeycomb-type lattice with the central nonmagnetic cations similar in size and equal in charge. The general formula for these compounds is $AAg_2(M'_{1/3}M_{2/3})[VO_4]_2$ where A = Sr^{2+}, Ba^{2+}, M′ = Mg^{2+}, Zn^{2+}, and M = Mn^{2+}(d^5, *S* = 5/2), Co^{2+} (d^7, *S* = 3/2), Ni^{2+} (d^8, *S* = 1) For simplicity, we will further refer to these compounds as

Received: January 6, 2014
Published: May 2, 2014

   dx.doi.org/10.1021/ic500028b | *Inorg. Chem.* 2014, 53, 4994−5001

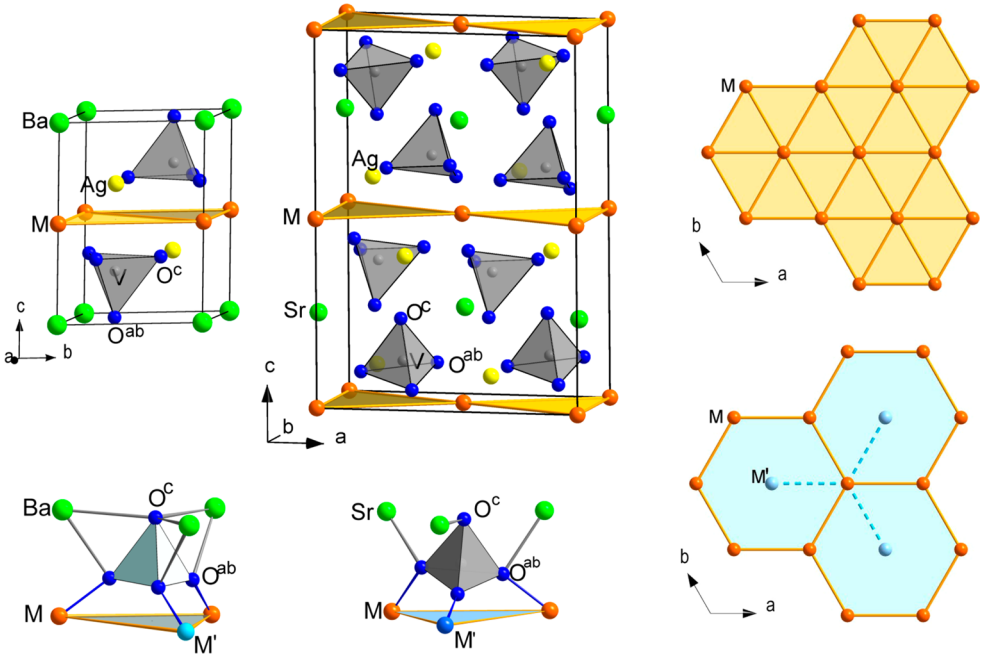

Figure 1. Crystal structures of $BaAg_2M[VO_4]_2$ ($P\bar{3}$; $Z = 1$) (left top) and $SrAg_2M[VO_4]_2$ ($C2/c$, $Z = 4$) (middle top). The M-site layer representing the magnetic cations on a triangular lattice (right top) and on a honeycomb lattice derivative: $M'_{1/3}M_{2/3}$ (right bottom). The connectivity of the $[VO_4]^{3-}$ unit in relation to $M'_{1/3}M_{2/3}$-sites on the honeycomb lattice is shown at the bottom left.

A(M′M), i.e., Ba(MgMn), where M′ is related to the 1/3 occupancy with a nonmagnetic ion and M to the 2/3 occupancy with a magnetic ion, respectively. The similarity of the divalent cations presents a challenge for obtaining homogenously distributed M/M′ ordering as required for the classification of a honeycomb lattice.

We will briefly discuss the crystal structure of these compounds, which are isotypic with structures previously reported.[27−29] Thermodynamic properties were measured and used to investigate the underlying magnetic properties of the respective honeycomb lattices. From theory, the number of magnetic nearest neighbors, z, and the exchange coupling parameter, J, both determine the Weiss constant, Θ, and the long-range order (LRO) critical temperature, T_C, in the following manner: $T_C \approx |\Theta| \sim \Sigma z_j|J_j|$.[30] The reduction in z enables us to evaluate the homogeneity of the metal cation distribution on the M-site in comparison with the respective triangular lattices.[1,3] Additionally, we have carried out lattice dynamic calculations and derived the lattice mode frequencies for each structure type reported here. On the basis of experimental Raman spectroscopic data and in particular the assignment of vanadate stretching modes, we show further proof of a homogeneous (local) distribution of M and M′.

2. EXPERIMENTAL SECTION

Powder samples of $AAg_2(M'_{1/3}M_{2/3})[VO_4]_2$ were prepared by ceramic solid-state techniques using ACO_3 (A = Ba^{2+} Matheson Coleman & Bell, Sr^{2+} Alfa Aesar), MCO_3 (M = Ni^{2+} Alfa Aesar, Co^{2+} Sigma-Aldrich, Mn^{2+} Alfa Aesar), MgO or ZnO (Alfa Aesar), and $AgVO_3$ (obtained by reacting Ag_2O Pfaltz & Bauer, Inc. and V_2O_5 Alfa Aesar). Note that $AgVO_3$ melts around 480 °C and may be considered as an internal flux to enhance the formation of homogeneous products. The starting materials for these compounds were mixed in the respective molar ratios, ground, and pressed into pellets. For the Ni^{2+} samples, a ball mill procedure (Zirconia container, 2 Zirconia balls, ground for 20 min on a SPEX Mixer/Mill 8000M) was used to increase the reactivity. The pelletized samples were heated in corundum crucibles in air at 550 °C for one day, then reground, repelletized, and heated again at 550 °C for one day. This process was repeated at least two times. The phase purity of the compounds was investigated by powder X-ray diffraction techniques (X'Pert Pro PANanalytical; Anton Paar, Cu-Kα_1 = 1.540 562 Å and -Kα_2 = 1.544 389 Å). The samples were ground and placed on a PW1817/32 zero background silicon crystal sample holder. The powder patterns were refined using the program system *FullProf*.[35] The program Diamond[36] was used to illustrate the crystal structures and lattices.

Further characterization includes spectroscopic, magnetization, and specific heat experiments. Midinfrared (MIR) data were collected at room temperature in reflectance mode with a Bruker Alpha-P FT on pure samples (not shown here). Raman spectra were performed on a Horiba Jobin Yvon T 6400 Spectrometer with an optical microscope, a liquid nitrogen cooled CCD detector and a laser excitation of Ar^+ (λ = 514.5 nm, 2.41 eV). Magnetic susceptibilities were measured with a Physical Property Measurement System (PPMS, Quantum Design) in the range of 2−300 K in both zero field (zfc) and field cooled (fc) mode in applied fields of up to 5 T. Field-dependent magnetization measurements were carried out in the temperature range from 2−20 K in applied field of up to 8 T. Specific heat measurements were performed in zero field and applied fields up to 5 T.

The first principle calculations of the electronic ground state of the $AAg_2M[VO_4]_2$ compounds with A = Ba^{2+}, Sr^{2+}, M = Mn^{2+}, Mg^{2+} were performed within the generalized gradient approximation using Perdew-Burke-Ernzerhof (PBE) local functional,[31] as implemented in the CASTEP code.[32] Norm-conserving pseudopotentials were used. Prior to performing lattice dynamics calculations, the structure was relaxed for the experimentally determined lattice parameters, so that forces on atoms in the equilibrium position did not exceed 3 meV/Å. The integration within the Brillouin zone was performed over a 3*3*2 Monkhorst-Pack grid[33] in the reciprocal space. Fixed electron occupancy constrains were imposed on the self-consistent field energy minimization as a prerequisite for using the variational density functional perturbation theory (linear response scheme) in the phonon calculations,[34] which treats the atomic displacements as perturbations.

dx.doi.org/10.1021/ic500028b | *Inorg. Chem.* 2014, 53, 4994−5001

3. RESULTS AND DISCUSSION

3.1. Crystal Structure. The crystal structures of the $AAg_2(M'_{1/3}M_{2/3})[VO_4]_2$ type of compounds are isotypic with $AAg_2Mn[VO_4]_2$ with A = Ba^{2+}, Sr^{2+}, respectively.[27,28] Figure 1 shows the two structure types that reflect the difference in the ionic radii, $r(Ba^{2+})$ = 1.35 Å and $r(Sr^{2+})$ = 1.18 Å.[37] The accompanying symmetry reduction from $P\bar{3}$ (Z = 1) to $C2/c$ (Z = 4) mainly causes a tilting of the $[VO_4]^{3-}$ unit and consequently a slight in-plane distortion (2-fold symmetry) of the planar M-site related 2D arrangement. In the $AAg_2M[VO_4]_2$ series the metal cations (M) are arranged on a triangular lattice where each M has six magnetic nearest neighbors. For the $AAg_2(M'_{1/3}M_{2/3})[VO_4]_2$ compounds, the metal cations are replaced in a 1:2 ratio of nonmagnetic to magnetic ions which may create a magnetic honeycomb-type lattice. In the honeycomb type of compounds, the magnetic metal ion is thus surrounded only by three nearest neighbor magnetic ions and three nonmagnetic ions (Figure 1). This reduction of the number of nearest neighbor magnetic ions, z, will eventually modify the magnetic properties. It is also important to note that the M-site of the compounds is linked exclusively through $[VO_4]^{3-}$ units via O^{ab} accountable for the supersuper exchange between the magnetic cations.

3.2. Powder X-ray Diffraction and Refinements. The lattice constants of the synthesized compounds were refined using the program *FullProf*,[35] see the Supporting Information, SI. In Figure 2, the refined powder pattern is shown for

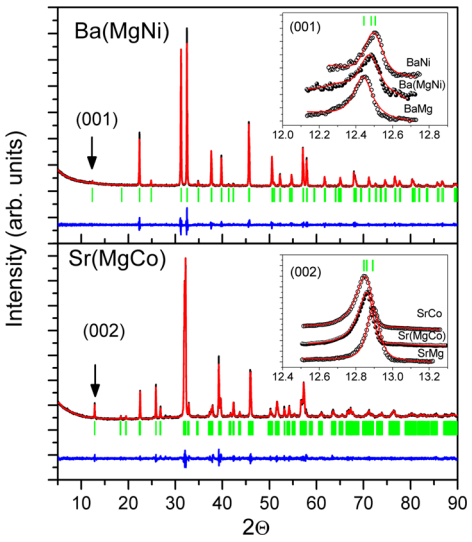

Figure 2. Main panels include the powder refinement patterns for Ba(MgNi) (top) and Sr(MgCo) (bottom). The insets give an overview of the single peak profile refinement of the honeycomb type of compounds in comparison with the parent triangular lattice type ones. Observed (black) and calculated (red) intensities/profiles, Bragg positions (green), and difference in intensity (blue). Refinements for the other compounds are shown in the SI.

Ba(MgNi) and Sr(MgCo), respectively. The insets include the single (001) and (002) Bragg reflections, respectively, in comparison with the parent compounds Ba(Mg), Ba(Ni), Sr(Mg), and Sr(Co) for reference. It is evident that the width of each profile is almost the same within each structure type and, more importantly, no splitting is observed. Thus, within the resolution limits, there is no evidence for a phase separation of the A(MgM)-type for the honeycomb-type of derivatives. Furthermore, the 2Θ position of A(MgM) reflects the respective ionic radii of the parent M-sites (triangular case) and the corresponding mixed occupancy on this M-site for the honeycomb type, well in line with the average ionic radii of a 1:2 ratio in the latter case. However, we note that no superstructure reflections were observed, which may indicate that the stacking of layers along [001] with different relative honeycomb-type orientations could be random.

Since the members of each series contain different cations on the M-site, which is mainly related to the *ab*-plane, we present the lattice constant a (A = Ba, $P\bar{3}$, Z = 1) and the derived averaged lattice constant $1/2(a^*+b)$ (A = Sr, $C2/c$ Z = 4) for the pseudohexagonal setting of the primitive unit cell ($a^* = 1/2(a^2+b^2)^{0.5}$) as a function of the respective ionic radii.[37] We note that the relationship observed here (see Figure 3) is well

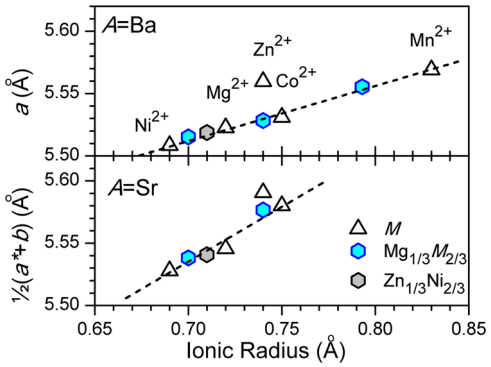

Figure 3. The dependence of the trigonal (A = Ba) and the transformed pseudohexagonal lattice constants $1/2(a^*+b)$ (A = Sr), respectively, on the ionic radii (M and $M'_{1/3}M_{2/3}$) are depicted for the triangular and honeycomb type of lattices. The dashed lines present a guide to the eye.

in line with a Vegard-law type of behavior.[38] However, the Zn-compound deviates from the general trend, which might be due to the cation's preference for tetrahedral coordination environments instead of the present octahedral one and thus leads to noticeable distortions within the layer.

3.3. Raman Spectroscopy and Lattice Dynamics. Raman spectra were collected for the honeycomb, $AAg_2(M'_{1/3}M_{2/3})[VO_4]_2$, and the parent triangular lattice, $AAg_2M[VO_4]_2$, compounds. DFT calculations were performed on the triangular lattice compounds. Here, Raman spectroscopy is used as a local probe: in the frequency range above 650 cm^{-1} the stretching modes of the $[VO_4]^{3-}$ unit are expected to occur, see also ref 39. For the honeycomb compounds, the surrounding of the $[VO_4]^{3-}$ unit is represented by one nonmagnetic ion (Zn^{2+} or Mg^{2+}) and two magnetic ions (Mn^{2+}, Co^{2+}, or Ni^{2+}), as shown in Figure 1.

First, we will discuss the Raman spectra of the $BaAg_2M[VO_4]_2$ family with M = Mn, ($Mg_{1/3}Mn_{2/3}$) and Mg as an example (Figure 4, left top panel). The calculated highest energy mode for this series of compounds is of A_g symmetry, and is due to the symmetric stretching, $\nu(V-O^c)$, of the $[VO_4]^{3-}$ unit toward the A-site layer ($A_g^{(6)}$ vibration). The position of the $A_g^{(6)}$ mode shows only a small shift between the set of the three compounds (parent compounds Ba(M) and honeycomb ones Ba(M′M)) since the *A*-site remains intact and is occupied by Ba^{2+}.

The next highest energy mode is a fully symmetric $A_g^{(5)}$ vibration. This mode represents the symmetric stretching of the

dx.doi.org/10.1021/ic500028b | Inorg. Chem. 2014, 53, 4994−5001

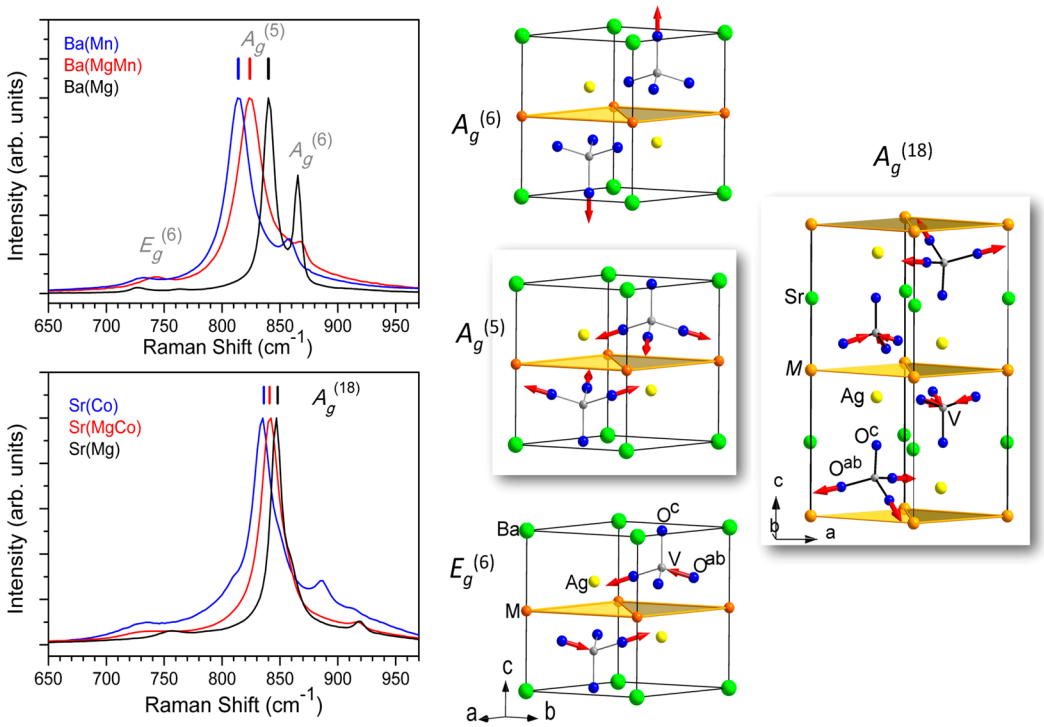

Figure 4. (Top left) Raman spectra of parent $BaAg_2M[VO_4]_2$ compounds with M = Mn (blue), Mg (black) in comparison with $BaAg_2(Mg_{1/3}Mn_{2/3})[VO_4]_2$ (red). The position of the most intense $A_g^{(5)}$ mode for each compound is marked. The assigned $A_g^{(6)}$ and $E_g^{(6)}$ modes are referenced. (Middle panel) The calculated displacements (red vectors) are shown for the $[VO_4]$ stretching modes $A_g^{(6)}$, $A_g^{(5)}$, and $E_g^{(6)}$ for the Ba-series. (Bottom left) Raman spectra of the parent $SrAg_2M[VO_4]_2$ compounds with M = Co (blue), Mg (black) in comparison with $SrAg_2(Mg_{1/3}Co_{2/3})[VO_4]_2$ (red). The position of the most intense $A_g^{(18)}$ mode for each compound is marked. (Right panel) The displacement pattern of the $A_g^{(18)}$ vibrational mode (for simplicity the reduced pseudohexagonal cell (A = Sr) is shown).

$[VO_4]^{3-}$ unit toward the M-site layer. Thus, this mode is expected to be the most sensitive to changes in the ionic radii of the M-site. Indeed, in the experimental spectra the energy of this mode $\nu(V-O^{ab})$, shows the largest shift (~30 cm^{-1}) between the three compounds of each set, as it shifts to higher wavenumbers with decreasing ionic radius. For the Ba(MgMn) compound, this shift nicely presents the 1:2 ratio with respect to the parent Ba(Mg) and Ba(Mn) compounds.

The third vibrational mode in the spectral range of interest is assigned to the $E_g^{(6)}$ mode, which represents the degenerate stretching, $\nu(V-O^{ab})$, of the $[VO_4]^{3-}$ unit toward the M-site layer. This assignment is also well supported by the expected fairly low intensity of this mode for all three compounds. Again, the total shift is rather small within the compounds of a set and not much altered with respect to variations in the transition metal series.

It is important to note that the magnetic members exhibit similar Raman line widths for each of the vibrational modes, a fact that signals the lack of disorder on the microscopic scale within the accessible scattering volume of several μm^3. This observation is consistent with the Bragg reflection single peak evaluation, shown in Figure 2, which indicates no significant difference in crystallinity as well. However, the Ba(Mg) modes are slightly sharper, and the energies between $A_g^{(6)}$ and $E_g^{(6)}$ are spanning over a wider region. One could speculate that this is reflecting the difference in bonding interaction between M–O^{ab}–V and Mg–O^{ab}–V. The former is more covalent, e.g., of a transition metal complex-type, while the latter is more ionic in character. Thus, the O^{ab}–V bonding is enforced (blue-shift) for the ionic case, see also below.

The total number of even-parity Raman-active modes is larger for the $SrAg_2M[VO_4]_2$ in comparison with $BaAg_2M[VO_4]_2$ compounds (38 versus 12, respectively) due to symmetry reduction and increase of formula units per unit cell ($C2/c$, $Z = 4$). Note here we show the reduced primitive pseudohexagonal unit cell with $Z = 2$, see Figure 4. One set of spectra (parent and honeycomb type of compounds) for the A = Sr case is shown in Figure 4 (left bottom panel). Overall, 19 Raman modes of A_g and 19 modes of B_g symmetry are allowed for this material. In the range of interest, (V–O) stretching, in total eight modes are expected to be active, six A_g and two B_g. $A_g^{(14-17)}$ results from the splitting of the $E_g^{(6)}$ mode (A = Ba case). $A_g^{(18)}$ presents the most intense mode and can be assigned to the totally symmetric (V–O^{ab}) stretching, thus resembling the above-discussed $A_g^{(5)}$ mode in the A = Ba case. Similarly, the pronounced shift of the $A_g^{(18)}$ mode relates well to the respective ions of the parent type of compounds and to the averaged ionic radii of the honeycomb one (see also Figure 5 for an overview). A shoulder that is observed at the high-frequency side of the $A_g^{(18)}$ mode, is assigned to the $B_g^{(18)}$ mode. The highest energy mode, $A_g^{(19)}$, is likewise comparable to the $A_g^{(6)}$ one (A = Ba case), and is due to the symmetric (V–O^c) stretching displacement. The related mode of the former type of displacement, $B_g^{(19)}$, is found at slightly lower energies. Further experimental details and computational results can be found in the SI.

It is interesting to note that overall, the phonon modes are slightly shifted to higher energies for A = Sr, which might be attributed to a chemical pressure effect on the vanadate induced by the smaller A-site cation, here Sr^{2+}. In fact, the reduced cell volume (V/Z) for the Sr-compounds is found to be smaller

dx.doi.org/10.1021/ic500028b | Inorg. Chem. 2014, 53, 4994–5001

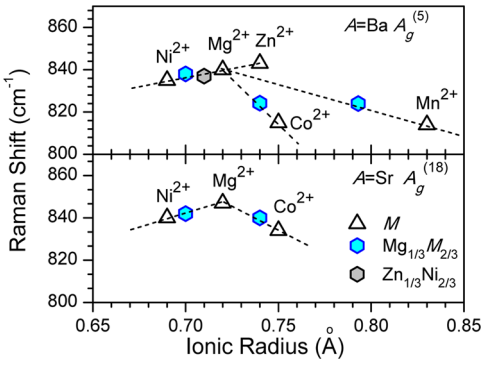

Figure 5. The dependence of the $A_g^{(5)}$ mode frequency (A = Ba) and the $A_g^{(18)}$ mode frequency (A = Sr) on the ionic radii (M and $M'_{1/3}M_{2/3}$) for the triangular and honeycomb type of lattices. The dashed lines present a guide to the eye.

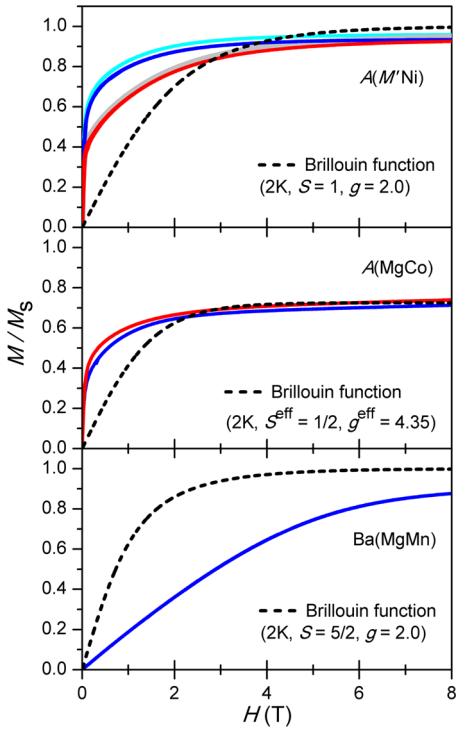

Figure 6. The normalized field-dependent magnetization (M/M_s) per magnetic ion at 2 K for A(M′Ni) (top), A(MgCo) (middle), and Ba(MgMn) (bottom). Blue: Ba(MgM); cyan: Ba(ZnNi); red: Sr(MgM); and gray: Sr(ZnNi). The dashed lines present the respective normalized magnetization for each paramagnetic spin system (Brillouin function) for comparison.

than the one for the Ba-case, see the SI. Furthermore, all modes (A = Sr) seem to be more narrow than those observed for A = Ba. From Figure 5, we may conclude that all presented honeycomb lattices are well in line with an average environment of one M′ and two M cations around each vanadate, see dashed lines connecting the parent triangular structures A(M) and the respective location of the A(M′M) compounds. We are showing the respective mode frequencies as a function of the ionic radii to emphasize the additional information that can be deduced from the Raman spectra.

Nonmagnetic compounds, A(Mg or Zn), exhibit higher energy modes than the magnetic ones for both A-site related series. This indicates weak covalence of the M−O bond, and consequently, the V−O^{ab} bonding is enhanced resulting in a blue-shift. The character of the magnetic M−O interaction being more covalent as typically observed in complexes requires electron density shifted from the V−O^{ab} bond toward the M-site, hence weakening the V−O^{ab} bond and inducing a red-shift in the spectra. The extent of this is obviously intrinsic to the magnetic M-cations, and therefore, no linear dependence on the ionic radii is observed, quite different from the above shown evaluation of X-ray data (Figure 3).

3.4. Thermodynamic Properties. The normalized field-dependent magnetization measurements, $M(H)/M_s$, are shown in Figure 6 and are compared to the respective Brillouin[40] function for each spin system. These Brillouin functions represent the behavior of the respective field dependent paramagnet at a specific temperature, here T = 2 K. The magnetization of the Ni-compounds exhibit a steeper response to the applied field than the Brillouin function for S = 1 and g = 2.0, which indicates ferromagnetic interactions. The Co-compounds are represented by a Brillouin function at T = 2 K for a single ion complex with an effective S^{eff} = 1/2 and g^{eff} = 4.35, for reference see the triangular lattice parent compounds.[1,3] Again, ferromagnetic correlations are apparent. Note that the hysteresis loop is very small and is not exceeding a width of 100 Oe. Furthermore, it is noticeable that there are only minor differences between the Ba and the Sr series for M = Co, but a significant decrease of M(H) is observed upon reaching the saturation value for the Sr(M′Ni) with respect to Ba(M′Ni) series. Contrary to these ferromagnetic cases, the Mn-compound exhibits an almost linear field dependence with a reduced magnetic moment, in comparison to the Brillouin function for an S = 5/2 system (g = 2.0). This suggests the presence of dominant antiferromagnetic correlations between the magnetic ions.

The inverse temperature dependent susceptibility (Figure 7) for the Ni-compounds follows a Curie−Weiss[40] law with a positive intersection on the temperature axis, again suggestive of dominant ferromagnetic correlations within the compound. For the A(M′Ni) series, an (averaged) Curie-constant, C, of 1.23 emuK/mol and Θ value of 3.6 K was determined. The Co-compounds follow a temperature dependent susceptibility that cannot be described by a typical Curie−Weiss behavior. Thus, the temperature dependence of the bulk susceptibility was calculated using the angular overlap model[41,42] for a single ion complex for comparison; see also ref 1. The inverse susceptibility of the Co-compounds intersects the temperature scale at ∼2.8 K, which can be associated with the respective Weiss temperatures, Θ, in an applied field. The reciprocal susceptibility of the Mn-compound exhibits a Curie−Weiss law type of behavior with C = 4.22 emuK/mol and Θ = −9.84 K, again corroborating the antiferromagnetic nature. The Neél temperature is expected below 2 K and cannot be reliably extracted from this data within the experimental range of this investigation. However, the ratio of $|\Theta|/T_N$ > 5 suggests a significant antiferromagnetic low-dimensional character. Note that for nearest neighbor interaction on a magnetic honeycomb lattice, frustration effects that would additionally lead to further suppression of long-range magnetic order are not expected.

Specific heat measurements were performed to investigate the long-range order and transition temperatures of the compounds. Figure 8 shows the specific heat divided by the temperature, $C_p(T)/T$, at zero field for Ba(M′Ni) as an example and includes the phonon contributions, $C_{lattice}(T)/T$,

dx.doi.org/10.1021/ic500028b | Inorg. Chem. 2014, 53, 4994−5001

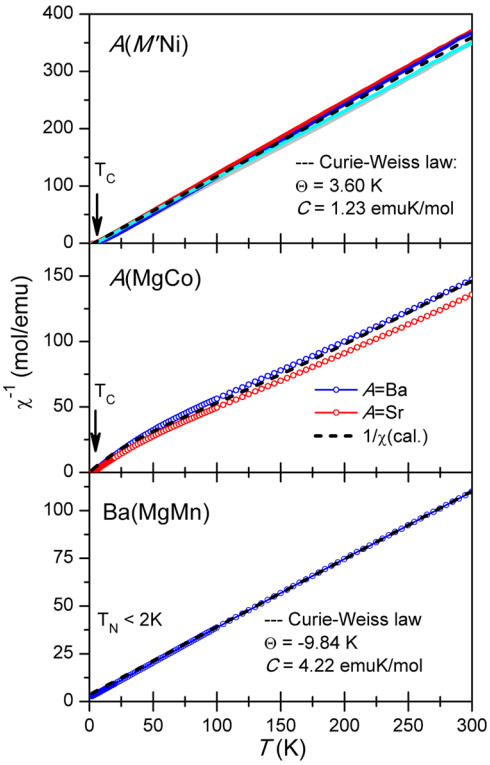

Figure 7. Inverse susceptibility data (applied field of 1000 Oe) for A(M′Ni) (top), A(MgCo) (middle), and Ba(MgMn) (bottom). Blue: Ba(MgM); cyan: Ba(ZnNi); red: Sr(MgM); and gray: Sr(ZnNi). The dashed black lines present fits to the Curie Weiss Law for M = Ni^{2+} and Mn^{2+}, and the calculated temperature dependence susceptibility of the single-ion complex, $[CoO_6]$, $S = 3/2$.

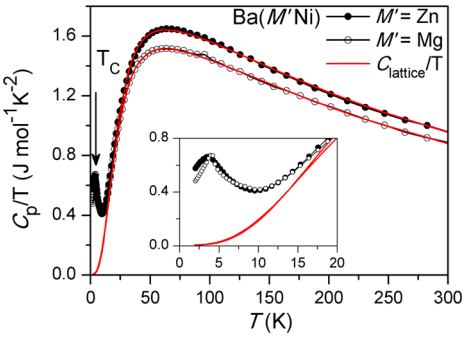

Figure 8. The specific heat divided by the temperature at zero field for Ba(MgNi) and Ba(ZnNi) compared to the respective phonon contribution (red). The λ-anomaly indicates the Curie temperature, T_C. The inset shows an enlargement of the low-temperature region. Specific heat data for the other compounds are given in the SI.

derived from the respective nonmagnetic parent compounds. The difference between the total specific heat and the phonon contribution then represents the magnetic part of the specific heat, $C_m(T)$. Integration of $C_m(T)/T$ (here: 2−50 K) provides the released spin entropy $S_m(T)$ in relation to the respective spin system, $R \ln(2S + 1)$, see the SI. The sharp λ-anomaly in the specific heat is indicative of a long-range order magnetic transition and exhibits dependence on the applied magnetic field, shown in Figure 9. From these evaluations, we can obtain T_C for the Ni-compounds and Co-compounds. The transition temperatures at zero applied fields are given in Table 1 for the

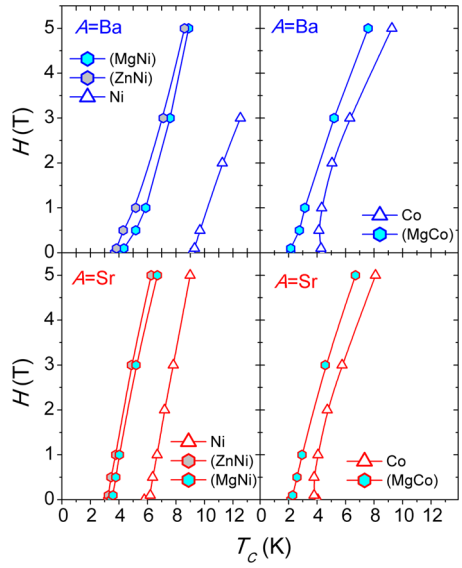

Figure 9. The field dependence of the respective Curie temperatures (T_C) is shown for the ferromagnetic honeycomb-type series A(MgM) and A(ZnNi) in comparison with the parent A(M) triangular lattice compounds.

magnetic honeycomb lattice compounds in comparison with the triangular lattice compounds.

Table 1. Comparison of Critical Temperatures T_C in K Obtained from the Specific Heat in Zero Applied Fields for $AAg_2(M)[VO_4]_2$, A(M), and $AAg_2(M'_{1/3}M_{2/3})[VO_4]_2$, A(M′M).

A(M)	T_C [1,3]	A(M′M)	T_C
Ba(Ni)	9.2	Ba(MgNi)	4.2
		Ba(ZnNi)	3.8
Sr(Ni)	6.0	Sr(MgNi)	3.5
		Sr(ZnNi)	3.2
Ba(Co)	4.2	Ba(MgCo)	2.2
Sr(Co)	4.2	Sr(MgCo)	2.2

From Table 1 and Figure 9, it can be seen that T_C for the ferromagnetic honeycomb-type of compounds are almost one-half of those for the triangular lattice type of compounds. This can be rationalized by the relationship $T_C \approx |\Theta| \sim \Sigma z_i|J_i|$.[30] Θ and T_C are both related to z (the number of nearest magnetic neighbors) and their magnetic exchange interactions, for further details, see also ref 43. In a first approximation, we neglect the contribution of the very weak interplanar magnetic interactions ($z^{inter}J^{inter}$), which should be orders of magnitude smaller than the intraplanar supersuper exchange couplings ($z^{intra}J^{intra}$) here, see also ref 1 for J^{intra}/J^{inter} for the triangular lattice Co-compounds. We recall from Figure 1 that $z^{TL} = 6$ for the triangular lattice and $z^{HL} = 3$ for the honeycomb type of compounds within the layer. Hence, the reduction of z^{intra} by a factor of 2 should thus cause a reduction of the transition temperature by ∼1/2. As a result, we may conclude that these observations indicate that for the ferromagnetic honeycomb-type compounds reported here the M-site is homogenously distributed in a 1:2 ratio of M′ (nonmagnetic, M′ = Mg or Zn) and M (magnetic, M = Ni, Co).

Additionally, the field dependence of T_C (Figure 9) of each compound reveals that with respect to the inherent spin-

dx.doi.org/10.1021/ic500028b | Inorg. Chem. 2014, 53, 4994−5001

systems representatives of different models are present. The Ni-compounds and Mn-compound are examples of a Heisenberg model with the magnetic moments in the *ab*-plane, see also ref 1 for the parent type of compounds which have been studied by neutron diffraction. The Co-compounds (S^{eff} = 1/2) are representatives of an Ising model with the magnetic moments of the spins orientated along the *c*-axis. Note that the magnetic interaction of the investigated compounds are of a supersuper exchange type exclusively via the bridging vanadates and can be sorted into two categories in relation to the electron configuration $3d^n$ (M): ferromagnets with $n > 5$ and antiferromagnets for $n \leq 5$.

4. CONCLUSIONS

A series of the magnetic honeycomb-type lattice, $AAg_2(M'_{1/3}M_{2/3})[VO_4]_2$, has been synthesized. From X-ray diffraction, it can be concluded that the compounds are isotypic to the parent triangular-type of compounds, $AAg_2M[VO_4]_2$, and that the compounds reported here appear to be single phase. Raman spectroscopy was used as a local probe of the $[VO_4]^{3-}$ structural unit environment. The Raman data support the homogeneous distribution of nonmagnetic to magnetic ion ratio of 1:2 inherent to the formation of a magnetic honeycomb lattice. Magnetic and specific heat measurements show that like the parent compounds, the Ni- and Co-compounds exhibit ferromagnetic correlations, whereas the Mn-compound is an antiferromagnet. Furthermore, the Curie temperature related to magnetic long-range order (λ-anomaly in the specific heat) is reduced by one-half for the honeycomb series with respect to the triangular parent type of ferromagnetic compounds. This one-half reduction of T_C originates from the reduction of the number of nearest neighbors, $z^{TL} = 6$ and $z^{HL} = 3$. Again, these findings, generated from the measurements of thermodynamic properties, indicate a homogeneous distribution of one nonmagnetic and two magnetic M-site ions and thus corroborate the successful synthesis of magnetic honeycomb-type lattices within the $AAg_2(M'_{1/3}M_{2/3})[VO_4]_2$ series.

■ ASSOCIATED CONTENT

Supporting Information

Refinement of XRD data; table of interatomic distances; Raman spectra; and specific heat data for the $AAg_2(M'_{1/3}M_{2/3})[VO_4]_2$ series. This material is available free of charge via the Internet at http://pubs.acs.org.

■ AUTHOR INFORMATION

Corresponding Author

*E-mail: amoeller@uh.edu

Notes

The authors declare no competing financial interest.

■ ACKNOWLEDGMENTS

This work has been supported by the NSF (Grant DMR-1149899) and by the State of Texas through the Texas Center for Superconductivity at the University of Houston.

■ REFERENCES

(1) Möller, A.; Amuneke, N. E.; Daniel, P.; Lorenz, B.; de la Cruz, C. R.; Gooch, M.; Chu, P. C. W. *Phys. Rev. B.* **2012**, *85*, 214422/1−13.
(2) Amuneke, N. E.; Gheorghe, D. E.; Lorenz, B.; Möller, A. *Inorg. Chem.* **2011**, *50*, 2207−2214.
(3) Amuneke, N. E. *Synthesis and Structure-Property Relationships of the $AAg_2M[VO_4]_2$ Type of Compounds*. PhD Dissertation, University of Houston: Houston, TX, August 2013.
(4) Tsirlin, A. A.; Möller, A.; Lorenz, B.; Skourski, Y.; Rosner, H. *Phys. Rev. B.* **2012**, *85*, 014401/1−8.
(5) Nakayama, G.; Hara, S.; Sato, H.; Narumi, Y.; Nojiri, H. *J. Phys. Condens. Matter* **2013**, *25*, 116003/1−8.
(6) Viciu, L; Huang, Q.; Morosan, E.; Zandbergen, H. W.; Greenbaum, N. I.; McQueen, T.; Cava, R. J. *J. Solid State Chem.* **2007**, *180*, 1060−1067.
(7) Regnault, L. P.; Burlet, P.; Rossat-Mignod, J. *Physica B* **1977**, *86*, 660−662.
(8) Shamoto, S.; Kato, T.; Ono, Y.; Miyazaki, Y.; Ohoyama, K.; Ohashi, M.; Yamaguchi, Y.; Kajitani, T. *Physica C* **1998**, *306*, 7−14.
(9) Bieringer, M.; Greedan, J. E.; Luke, G. M. *Phys. Rev. B* **2000**, *62*, 6521−6529.
(10) (a) Berthelot, R.; Schmidt, W.; Muir, S.; Eilertson, J.; Etienne, L.; Sleight, A. W.; Subramanian, M. A. *Inorg. Chem.* **2012**, *51*, 5377−5385. (b) Schmidt, W.; Berthelot, R.; Sleight, A. W.; Subramanian, M. A. *J. Solid State Chem.* **2013**, *201*, 178−185. (c) Seibel, E. M.; Roudebush, J. H.; Wu, H.; Huang, Q.; Ali, M. N.; Ji, H.; Cava, R. J. *Inorg. Chem.* **2013**, *52*, 13605−13611. (d) Roudebush, J. H.; Andersen, N. H.; Ramlau, R.; Garlea, V. O.; Toft-Petersen, R.; Norby, P.; Schneider, R.; Hay, J. N.; Cava, R. J. *Inorg. Chem.* **2013**, *52*, 13605−13611.
(11) Möller, A.; Löw, U.; Taetz, T.; Kriener, M.; André, G.; Damay, F.; Heyer, O.; Braden, M.; Mydosh, J. A. *Phys. Rev. B.* **2008**, *78*, 024420/1−10.
(12) Yehia, M.; Vavilova, E.; Möller, A.; Taetz, T.; Löw, U.; Klingeler, R.; Kataev, V.; Büchner, B. *Phys. Rev. B.* **2010**, *81*, 060414/1−4.
(13) Kataev, V.; Möller, A.; Löw, U.; Jung, W.; Schittner, N.; Kriener, M.; Freimuth, A. *J. Magn. Magn. Mater.* **2005**, *290*, 310−313.
(14) Rogado, N.; Huang, Q.; Lynn, J. W.; Ramirez, A. P.; Huse, D.; Cava, R. J. *Phys. Rev. B.* **2002**, *65*, 144443/1−7.
(15) Regnault, L. P.; Henry, J. Y.; Rossat-Mignod, J.; De Combarieu, A. *J. Magn. Magn. Mater.* **1980**, *15*, 1021−1022.
(16) Wichmann, R.; Müller-Buschbaum, H. *Rev. Chim. Miner.* **1984**, *21*, 824−830.
(17) Hagemann, I. S.; Huang, Q.; Gao, X. P. A.; Ramirez, A. P.; Cava, R. J. *Phys. Rev. Lett.* **2001**, *86*, 894−897.
(18) Sachdev, S. *Phys. Rev. B* **1992**, *45*, 12377−12396.
(19) Goodenough, J. B. *Magnetism and the Chemical Bond*; Wiley: Cambridge, MA, 1963.
(20) Kanamori, J. *J. Phys. Chem. Solids* **1959**, *10*, 87−98.
(21) de Jongh, L. J.; Miedema, A. R. *Adv. Phys.* **2001**, *50*, 947−1170.
(22) Koo, H.-J.; Whangbo, M.-H. *Inorg. Chem.* **2006**, *45*, 4440−4447.
(23) Whangbo, M.-H.; Koo, H.-J.; Dai, D. *J. Solid State Chem.* **2003**, *176*, 417−481.
(24) Wadati, H.; Kato, K.; Wakisaka, Y.; Sudayama, T.; Hawthorn, D. G.; Regier, T. Z.; Onishi, N.; Azuma, M.; Shimakawa, Y.; Mizokawa, T.; Tanaka, A.; Sawatzky, G. A. *Solid State Commun.* **2013**, *162*, 18−22.
(25) Han, T.-H.; Helton, J. S.; Chu, S.; Nocera, D. G.; Rodriguez-Rivera, J. A.; Broholm, C.; Lee, Y. S. *Nature* **2012**, *492*, 406−410.
(26) Misguich, G.; Lhuillier, C. *Frustrated Spin Systems*; World Scientific: Singapore, 2004.
(27) Rettich, R.; Müller-Buschbaum, H. *Z. Naturforsch. B* **1998**, *53*, 291−295.
(28) Rettich, R.; Müller-Buschbaum, H. *Z. Naturforsch. B* **1998**, *53*, 279−282.
(29) von Postel, M.; Müller-Buschbaum, H. *Z. Anorg. Allg. Chem.* **1992**, *618*, 107−110.
(30) Kittel, C. *Introduction to Solid State Physics*, 8th ed.; John Wiley and Sons, Inc.: New York, 2005.
(31) Perdew, J. P.; Burke, K.; Ernzerhof, M. *Phys. Rev. Lett.* **1996**, *77*, 3865−3868.
(32) Clark, S. J.; Segall, M. D.; Pickard, C. J.; Hasnip, P. J.; Probert, M. I. J.; Refson, K.; Payne, M. C. *Z. Kristallogr.* **2005**, *220*, 567−570.
(33) Monkhorst, H. J.; Pack, J. D. *Phys. Rev. B* **1976**, *13*, 5188−5192.

(34) Refson, K.; Tulip, P. R.; Clark, S. J. *Phys. Rev. B* **2006**, *73*, 155114/1−12.
(35) Rodriguez-Cavajal, J. *FullProf 2000* V. 4.80; Laboratoire Léon Brillouin CEA-CNRS: Gif-sur-Yvette, Cedex, Franceavailable at http://www.ill.eu/sites/fullprof/, 2009.
(36) Brandenburg, K. *Diamond* V. 3.2e; Crystal Impact GbR: Bonn, Germany, 1997−2010.
(37) (a) Shannon, R. D.; Prewitt, C. T. *Acta Crystallogr. B* **1969**, *25*, 925−946. (b) Shannon, R. D. *Acta Crystallogr. A* **1976**, *32*, 751−767.
(38) Vegard, L. *Z. Phys. A. Hadrons Nucl.* **1921**, *5*, 17−27.
(39) Kimani, M. M.; Thompson, L.; Snider, W.; McMillen, C. D.; Kolis, J. W. *Inorg. Chem.* **2012**, *51*, 13271−13280.
(40) (a) Kahn, O. *Molecular Magnetism*; Wiley-VCH: Weinheim, 1993. (b) Orchard, A. F. *Magnetochemistry*; Oxford University Press: Oxford, U.K., 2003.
(41) Schäffer, C. E.; Jørgensen, C. K. *Mol. Phys.* **1965**, *9*, 401−412.
(42) (a) Riley, M. *CAMMAG for PC*, V. 4.0;University of Queensland: St. Lucia, Australia, 1997; (b) Gerloch, M. *Magnetism and Ligand-Field Analysis*: Cambridge University Press: Cambridge, U.K., 1983; (c) Gerloch, M.; McMeeking, R. F. *J. Chem. Soc. (Dalton)* **1975**, 2443−2451.
(43) de Jongh, L. J. *Magnetic Properties of Layered Transition Metal Compounds*; Kluwer Academic Publishers: Dordrecht, Boston, 1990.